The link between brushite and gypsum: Miscibility, dehydration and crystallochemical behavior in the CaHPO4.2H2O-CaSO4.2H2O system

Journal:	*Crystal Growth & Design*
Manuscript ID:	cg-2011-012815.R2
Manuscript Type:	Article
Date Submitted by the Author:	09-Nov-2011

Complete List of Authors:	Pinto, Andre; Universidade de Lisboa, Geologia Carneiro, Joana; Universidad de Oviedo, Geologia Katsikopoulos, Dionisis; Universidad de Oviedo, Geologia Jimenez, Amalia; Universidad de Oviedo, Geologia Prieto, Manuel; Universidad de Oviedo, Geologia

The link between brushite and gypsum: Miscibility, dehydration and crystallochemical behavior in the $CaHPO_4{\cdot}2H_2O$-$CaSO_4{\cdot}2H_2O$ system

André J. Pinto, Joana Carneiro, Dionisis Katsikopoulos, Amalia Jiménez* and Manuel Prieto.
Dpto. de Geología, Universidad de Oviedo, C/ Arias Velasco s/n, 3305 Oviedo, Spain

The present study explores the mixing properties of the $Ca(SO_4,HPO_4){\cdot}2H_2O$ solid solution and the role of the "double-salt" $Ca_2SO_4HPO_4{\cdot}4H_2O$ (ardealite) by means of precipitation experiments carried out in a solution calorimeter at 25ºC. Moreover, the dehydration behavior of a number of solids with different compositions is studied by thermogravimetry and thermo-X-ray diffraction. The experimental results indicate the existence of two (sulfate-rich and phosphate-rich) ranges of solid solution which are separated by two miscibility gaps from a range around the midpoint (~50% molar) composition in which ardealite forms. On the phosphate-rich miscibility range, the structural (020) layers contract with the sulfate content, whereas the interlayer spacing expands. This contraction is consistent with the negative enthalpy of mixing determined from the calorimetric data. For the ardealite range of compositions, the strong contraction of the (020) layers resolves in a different stacking sequence (with double *b*-axis and (040) as elementary stacking layers). Therefore, ardealite is demonstrated to be not a member of the $Ca(SO_4,HPO_4){\cdot}2H_2O$ solid solution, but a nearly stoichiometric compound with specific structural features. The thermogravimetric study indicates a specific dehydration behavior for ardealite, which again supports the idea that this phase is not a member of the solid solution.

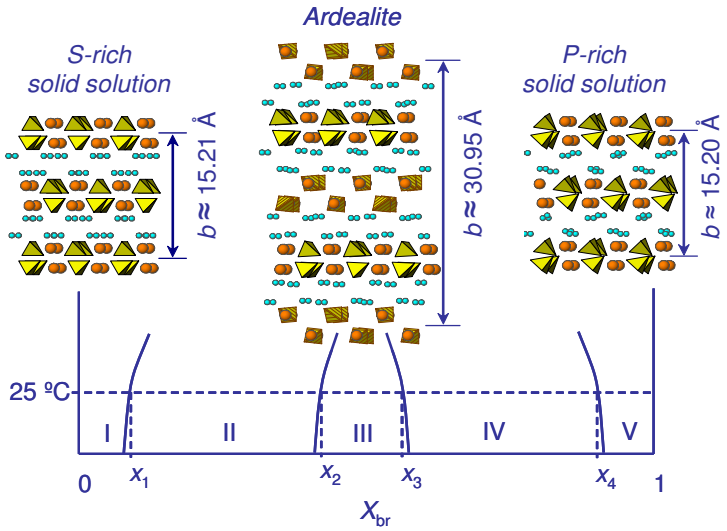

Figure: Scheme of the distribution of phases in the $CaSO_4{\cdot}2H_2O$-$CaHPO_4{\cdot}2H_2O$ system that includes the projection of 101 slices of the structures of ardealite and of the two extremes of the $Ca(SO_4,HPO_4){\cdot}2H_2O$ solid solution. In the case of ardealite[24], there are two topologically non-equivalent tetrahedral positions (striped and non-striped tetrahedra). In all cases, the small circles represent oxygen atoms from the water molecules. The larger circles represent the calcium atoms. The solid lines separate the hypothetical stability fields of the different phases described in the text.

**Corresponding author:*

Amalia Jiménez
C/ Jesus Arias de Velasco s/n.
33005 Oviedo, Spain
Tel. (+34) 985 109552. Fax. (+34) 985 103 103.
amjimenez@uniovi.es

The link between brushite and gypsum: Miscibility, dehydration and crystallochemical behavior in the $CaHPO_4 \cdot 2H_2O$-$CaSO_4 \cdot 2H_2O$ system

André J. Pinto[1], Joana Carneiro, Dionisis Katsikopoulos, Amalia Jiménez* and Manuel Prieto

Departamento de Geología, Universidad de Oviedo, C/ Arias Velasco s/n, 3305 Oviedo, Spain

* Corresponding author: *amjimenez@uniovi.es*

[1] Present address: Andre J. Pinto. Departamento de Geologia, Faculdade de Ciências da Universidade de Lisboa. Edifício C6, Campo Grande, 1749-016 Lisboa, Portugal.

ABSTRACT

The present study explores the mixing properties of the $Ca(SO_4,HPO_4)\cdot 2H_2O$ solid solution and the role of the "double-salt" $Ca_2SO_4HPO_4\cdot 4H_2O$ (ardealite) by means of precipitation experiments carried out in a solution calorimeter at 25ºC. Moreover, the dehydration behavior of a number of solids with different compositions is studied by thermogravimetry and thermo-X-ray diffraction. The experimental results indicate the existence of two (sulfate-rich and phosphate-rich) ranges of solid solution which are separated by two miscibility gaps from a range around the midpoint (~50% molar) composition in which ardealite forms. On the phosphate-rich miscibility range, the structural (020) layers contract with the sulfate content, whereas the interlayer spacing expands. This contraction is consistent with the negative enthalpy of mixing determined from the calorimetric data. For the ardealite range of compositions, the strong contraction of the (020) layers resolves in a different stacking sequence (with double *b*-axis and (040) as elementary stacking layers). Therefore, ardealite is demonstrated to be not a member of the $Ca(SO_4,HPO_4)\cdot 2H_2O$ solid solution, but a nearly stoichiometric compound with specific structural features. The thermogravimetric study indicates a specific dehydration behavior for ardealite, which again supports the idea that this phase is not a member of the solid solution.

1. INTRODUCTION

Phosphate minerals are not particularly abundant in the Earth's crust, but they are of significant importance in biogeochemical processes that occur in both marine and terrestrial environments. Lamentably, high concentrations of phosphates in natural waters can lead to the increased growth of green algae, triggering a process known as eutrophication, which usually deteriorates the aquatic environment. The excessive use of phosphate-based fertilizers to sustain food production at a global scale has recently raised the question of how to recycle our very limited phosphorus resources and reduce their environmental impact at the same time[1]. The major exploitable reserves of phosphorous occur in the form of calcium phosphates, mainly minerals of the apatite group, which have been

extensively investigated because of their relevance in biomineralization, materials and environmental sciences[2,3]. Another calcium phosphate, brushite $CaHPO_4 \cdot 2H_2O$, has received increasing attention due to its significance in technological and environmental issues [4-6]. Brushite is a major component of kidney and bladder stones and is widely used as a coating for bone implants[7]. Moreover, this mineral has been proposed as a precursor of hydroxylapatite $Ca_5(PO_4)_3OH$ in many natural processes[8], including the formation of bones and teeth[9]. In the environment, brushite occurs mainly in deposits of phosphorites[10], caves and other P-rich media, such as fertilized soils[11]. Brushite coexists commonly with gypsum in many of these natural deposits[12] and also in some industrial wastewater products[13]. In fact, the existence of a relationship between these two minerals was first documented by Schadler[14], who reported the presence of a mineral called ardealite $Ca_2HPO_4SO_4 \cdot 4H_2O$ in cave deposits where brushite and gypsum occur together. However, despite this early reference, the factors controlling the co-precipitation of brushite and gypsum from aqueous solutions and the crystallochemical role of ardealite (particularly the question of whether ardealite is a differentiated stoichiometric solid or a member of the $Ca_2(HPO_4,SO_4) \cdot 4H_2O$ solid solution) require further assessment.

When two chemically and structurally related compounds precipitate from a supersaturated aqueous solution, the formation of a solid solution is always a possibility, which holds true for cases other than that of cationic substitutions. The formation of solid solutions involving oxyanions like SO_4^{2-}, PO_4^{3-}, AsO_4^{3-}, SeO_4^{2-}, CrO_4^{2-}, and MoO_4^{2-} has been explored by a number of authors[15-17] due to the implications of these systems in nuclear waste disposal and other environmental issues. In the case of gypsum, the structural similarity with brushite and pharmacolite $CaHAsO_4 \cdot 2H_2O$ was considered in depth by Heijnen and Hartman[18], who presented a comparative study of their crystal morphologies using an *A*-setting for the three unit cells. More recent papers[19-22] illustrates how this structural similarity favors the development of oriented intergrowths between these three minerals. In the case of brushite and gypsum, the possibility of co-precipitation to form solid solution crystals

with anionic SO_4^{2-}/HPO_4^{2-} substitution was pointed out by a number of authors[23-24], but an evaluation of the extent and character of this solid solution has yet to be performed.

Brushite and gypsum have nearly identical unit cells, although due to the protonation of one of the oxygen atoms in the phosphate ion and to a different configuration of the water molecules, the spatial group (for a discussion on the unit-cell choice, see section 3.1) of brushite is $A1a1$ (No. 9), while gypsum crystallizes in $A12/a1$ (No. 15). The relation between the two crystal structures is reflected in the presence, or lack, of a 2-fold rotation axis along [010] and a symmetry center. As a consequence, brushite can grow onto gypsum following two alternative epitaxial orientations related by a 2-fold rotation axis[21]. Ardealite crystallizes in the same spatial group than brushite (No. 9) with similar *a* and *c* parameters (see section 3.1), but the *b*-axis periodicity is considered to be about twice (~30.95 > 2×15.180 Å) as long as that of brushite.

Like gypsum and brushite, natural and synthetic ardealites have a layered structure parallel to (010). However, the occurrence of $0k0$ X-ray reflections only with $k = 4n$ suggests that the periodicity along the *b*-axis in ardealite occurs at four times the elementary stacking layer[25], whereas in gypsum and brushite the repetition occurs every two layers. In fact, most evidence indicates that ardealite cannot be considered an intermediate member of the $Ca(SO_4,HPO_4)\cdot 2H_2O$ solid solution, but a virtually stoichiometric double salt with specific structural features. The presence of some SO_4^{2-}/HPO_4^{2-} ordering involving alternating layers along the *b*-axis is, however, more than doubtful. Several differences in the structural parameters (structure factor multiplicities, mean *T*-O bond lengths, etc.) concerning the tetrahedral [TO_4] groups in alternate (040) layers were identified in a synthetic ardealite-like phase[25]. However, given the small value of these differences, Sakae and co-workers[25] considered the SO_4^{2-}/HPO_4^{2-} distribution to be essentially random. In the model used by these authors, all of the contrasting layers are chemically analogous, but the mode of stacking occurs in such a way that the repeating period includes four layers. The question of whether or not the compounds synthesized[25] and natural ardealites are identical is not completely resolved, but it does seem likely.

Dehydration studies can offer an additional tool to further understand the differences between ardealite-like phases and gypsum-brushite solid-solution members. Since Linck and Jung[26] first described the nature of the gypsum dehydration products, the dehydration behavior of natural gypsum, phosphogypsum, and synthetic gypsum has been widely studied in the literature [27, 28]. It is worth noting the essential consistency among the existing data, despite the wide variety of techniques applied to these studies. After past discussion[29,30] regarding the possible formation of several intermediate hydrates with a number of water molecules other than 0.5 per formula unit, Putnis and co-workers[31] gathered *in situ* evidence for the formation of only the hemihydrate bassanite $CaSO_4 \cdot 0.5H_2O$ using infrared spectroscopy combined with thermogravimetry. The structure of the low-temperature (T < 383 K) dehydration products of gypsum ($CaSO_4 \cdot 0.5H_2O$ and γ-$CaSO_4$) was studied using time-of-flight neutron powder diffraction data[32]. Clarifying the pioneer studies[33,34], these authors conclude that, even though bassanite presents an overall structure very similar to γ-$CaSO_4$ ($P6_222$, S.G. No. 180), its diffraction patterns are consistent not with a trigonal, but with a monoclinic ($I2$, S.G. No.5) structure. Nevertheless, there are only minor arrangements in the crystal structure when bassanite dehydrates at low temperature to form γ-$CaSO_4$ (also known as the soluble anhydrite or III phase).

In contrast with gypsum, the dehydration behavior of brushite has not elicited a similar abundance of references[35,36]. Moreover, with the exception of a recent paper by Frost and co-workers[37] describing the thermal stability of a natural ardealite sample, there is no detailed study on the dehydration behavior of intermediate members in the gypsum-brushite joint. In this framework, the objectives of the present work were to (i) explore the mixing properties and assess the extent of the $Ca(SO_4,HPO_4)\cdot 2H_2O$ solid solution at ambient temperature, (ii) evaluate the presence of miscibility gaps and the crystallochemical role of ardealite in the gypsum-brushite joint, and (iii) describe the dehydration behavior of a number of solid phases with different compositions in this series. With this aim, we carried out a combined study involving solution calorimetry, thermogravimetry, thermo-XRD in solids formed via precipitation experiments.

2. EXPERIMENTAL METHODS

2.1. Solution calorimetry

The enthalpy of mixing of different members of the $Ca(SO_4,HPO_4)\cdot 2H_2O$ solid solution was studied by solution calorimetry following a protocol previously described in the literature[38,39]. Precipitation experiments were performed in the Dewar flask of a PARR6755 solution calorimeter equipped with a PARR 6772 high-precision thermometer. The Dewar flask was filled with 100 ml of a series of aqueous solutions containing dissolved Na_2SO_4-H_3PO_4 with different SO_4^{2-}/HPO_4^{2-} ratios (Table 1). These aqueous solutions were adjusted to pH 5.5 with the addition of NaOH and were left to cool for three hours at 25ºC until the heat of dilution of the NaOH had completely dissipated. Next, a glass cell containing 10 ml of a 1 M $CaCl_2$ aqueous solution sealed with a detachable Teflon cap was immersed in the Dewar flask and continuously rotated by an external electric motor. As soon as thermal equilibrium was reached, the glass cell was opened, and the reactants were mixed in the Dewar flask, where precipitation occurred. The changes in temperature associated with the precipitate formation were measured and recorded by a PARR 6772 precision thermometer. All experiments were performed in quintuplicate in a thermostated cabinet (25 ± 0.5 ºC) using deionized (MilliQ) water and analytical grade reagents.

Table 1. Initial concentrations of Na_2SO_4 and H_3PO_4 used in the experiments

Sample	Na_2SO_4(M)	H_3PO_4 (M)
C1	0.50	-
C2	0.50	0.10
C3	0.50	0.15
C4	0.50	0.20
C5	0.50	0.25
C6	0.50	0.30
C7	0.50	0.35
C8	0.50	0.40
C9	0.25	0.50
C10	0.20	0.50
C11	0.15	0.50
C12	-	0.50

2.2. Characterization of solids and aqueous solutions

The precipitates formed in the Dewar flask were extracted from the aqueous solution using 0.65 μm filters (Millipore) and left to dry at room temperature to avoid dehydration of the formed phases. Next, the solids were characterized by powder X-ray diffraction (XRD). The diffraction patterns were scanned from 5º to 80º (2θ) with a step size of 0.02º on a Philips X'Pert Pro automatic diffractometer using CuKα radiation. Between successive measurements, the diffractometer was calibrated using a silicon (Si) external standard. The diffractograms were studied using X'Pert HighScore Plus (©2008, PANalytical B.V.) to index the main reflections and calculate the cell parameters of each precipitate. Obviously, this method allows for recognizing the cases in which not a single phase but a mixture of different solid phases was formed. Moreover, the compositional homogeneity of the solids was checked by studying the full width at half maximum (FWHM) values of the main reflections.

The aqueous solutions were analyzed with an iCAP 6000 (Thermo) Inductively Coupled Plasma - Atomic Emission Spectrometer (ICP-AES). The mass and composition, expressed in terms of the brushite mole fraction ($X_{br} = 1-X_{gy}$) of each homogeneous (single-phase) precipitate, were determined from the initial and final (before and after precipitation) concentrations of sulfate and phosphate in the aqueous solution. Furthermore, representative samples of each precipitate were analyzed using a JEOL-6100 scanning electron microscope (SEM) equipped with an INCA Energy 200 microanalysis system (EDS), and the results were found to be in good agreement with the values derived from the solution compositions. However, the compositions derived from the ICP-AES analyses were more accurate (SD of $X_{br} \approx \pm 0.01$) than the EDS measurements and thus were chosen for subsequent calculations.

2.3 Thermogravimetry and Thermo-XRD

Thermogravimetric analyses (TG) of the precipitates obtained in the calorimeter were carried out using a Metter Toledo Me/TG thermal analyzer. Only the precipitates consisting of a single

phase were studied. All measurements were performed in the 293–650 K temperature range at a heating rate of 5 $K \cdot min^{-1}$ in an inert N_2 atmosphere. The initial mass of each sample was ~10 mg. The temperature precision of the equipment was ±0.25 K, and the weight precision was ±1 μg.

The dehydration of the single-phase precipitates was also studied by in situ thermo-XRD using CuKα radiation on a PANalytical X'PERT PRO powder diffractometer equipped with a PIXcel solid-state detector and a high temperature chamber (Anton Paar HTK 1200 N). The diffractograms were scanned over a $5 < 2\theta < 40^{\circ}$ range with a step size of 0.013º and a time step of 23.97 s. All measurements were performed in air by collecting the diffraction patterns at fixed temperatures (typically at 25 or 10 K increments) between 298 and 723 K. The heating rate between two consecutive scans was 5 $K \cdot min^{-1}$. The phase transformations were simply detected by the appearance and disappearance of characteristic reflections in the XRD patterns.

3. RESULTS AND DISCUSSION

3.1. Composition and mineralogical features of the precipitates

The powder XRD study revealed that the precipitates obtained in experiments C3, C4, and C8 (see Table 1) were not composed of a single solid phase, but rather of a mixture of two phases. For the rest of the experiments, the precipitates consisted of a single, compositionally homogeneous solid phase. A number of these precipitates (C2, C9, C10, and C11) were confirmed to be intermediate members of the $Ca(SO_4,HPO_4)\cdot 2H_2O$ solid solution, while precipitates C5, C6, and C7 were identified as an ardealite-like ($Ca_2SO_4HPO_4\cdot 4H_2O$) phase. Finally, as expected, the diffractograms of precipitates C1 and C12 (see Table 1) matched the reference diffraction patterns of pure gypsum (PDF 33-0311) and brushite (PDF 009-0077), respectively.

Figure 1 shows the indexed diffraction patterns of gypsum, brushite and intermediate members of the $Ca(SO_4,HPO_4)\cdot 2H_2O$ solid solution using an *A*-centered unit cell setting[18]. These authors used *A*12/*a*1 and *A*1*a*1 space group settings for describing the structure of gypsum and brushite, as this choice of unit cell enables the coincidence of the structural and the morphological *c*-axis of gypsum.

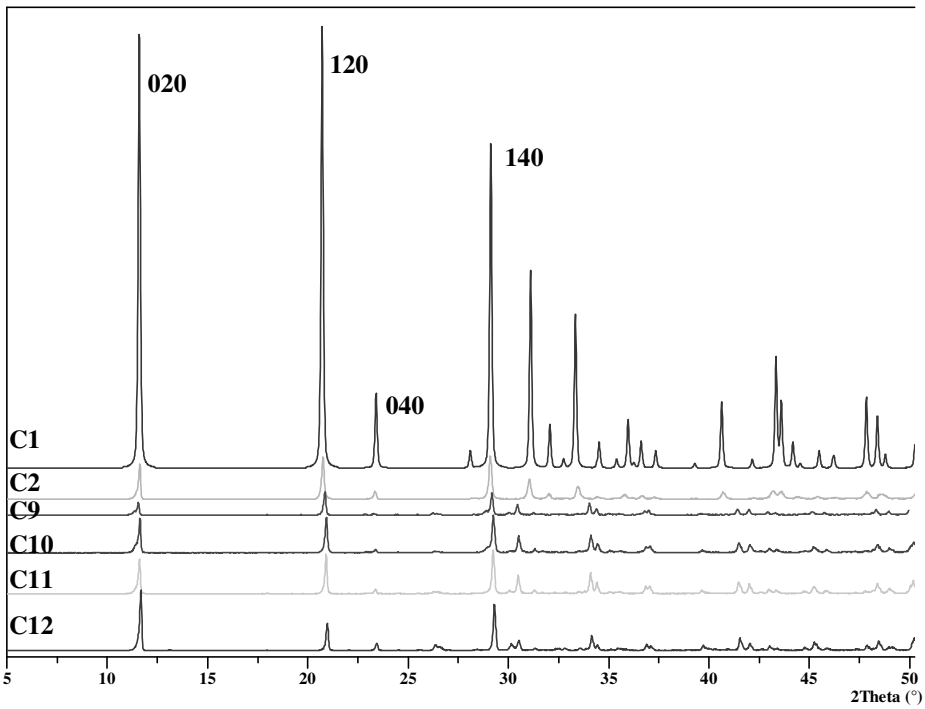

Figure 1. Powder diffraction patterns of gypsum (C1), brushite (C12) and several intermediate members (C2, C9, C10, and C11) of the $Ca(SO_4,HPO_4)\cdot 2H_2O$ solid solution. The reflections have been indexed using an *A*-centered unit cell setting (see text).

The relationships between both crystal structures have been widely described in a previous paper[21]. Gypsum crystallizes in the centrosymmetric point group *2/m* (without polar directions in its structure) and brushite crystallizes in the non-centrosymmetric point group *m*. Therefore, the space group of brushite (*A*1*a*1) is a subgroup of that of gypsum (*A*12/*a*1). Using these space group settings, the main reflections in the diffractogram of pure gypsum (C1) can be indexed as 020, 120, 040, and 140, (at *d*-spacings of ~7.60, 4.29, 3.80, and 3.07 Å, respectively). The main reflections are similar in the case of pure brushite (C12), with spacings that are slightly different (the unit cell volume is slightly smaller) from those of gypsum (~7.58, 4.24, 3.80, and 3.05 Å, respectively). By comparing diffractograms C2, C9, C10, and C11 with those of the pure end-members, it is clear that these samples correspond to intermediate members of the $Ca(SO_4,HPO_4)\cdot 2H_2O$ solid solution (see Fig. 1). For instance, diffractogram C2 shows reflections at ~7.62, 4.28, 3.81, and 3.07 Å, with the 020 spacing slightly larger than that of pure gypsum. Similarly, diffractograms C9, C10, and C11 are similar to that of brushite. The highest difference occurs in the case of C9, which shows

spacings significantly larger (~7.66, 4.26, 3.81, and 3.06 Å) than brushite. The precipitates were checked for compositional homogeneity by considering the broadening of a given reflection with respect to the width of the corresponding reflections in the diffractograms of the pure end-members[16]. Working with 020, i.e., the reflection with the largest *d*-spacing, the FWHM value was 0.097 (º2θ) for pure $CaSO_4{\cdot}2H_2O$ and 0.124 (º2θ) for pure $CaHPO_4{\cdot}2H_2O$.

The diffractograms of intermediate members of the solid solution show excess broadening with respect to the linear trend determined by the FWHM values of the end-members, but the deviations are relatively small. The maximum deviation (0.029º2θ) occurs for the 020 reflection in C9. Therefore, compositional heterogeneities (due either to the presence of relatively S- and P-enriched microdomains within each single crystal or to the coexistence of microcrystals with different compositions), if they exist, do not seem to be very significant. Table 2 shows the lattice parameters calculated (using X'Pert HighScore Plus) from these diffractograms. While the unit cell dimensions *a* and *c* are smaller in gypsum (C1), the parameter *b* and the cell volume are smaller in brushite (C12). Moreover, the evolution of the lattice parameters with composition is not monotonic. As we will see later, the *b*-axis is larger for intermediate compositions than for both end-members, and the unit cell dimensions do not change in a simple way along *a* and *c*.

Table 2. Calculated unit cell parameters (*A* unit-cell setting) of the samples identified as members of the $Ca(SO_4,HPO_4){\cdot}2H_2O$ solid solution.

Sample	*a* (Å)	*b*(Å)	*c*(Å)	□	V_{cell} (Å^3)
C1	5.675	15.214	6.284	114.06	495.45
C2	5.681	15.231	6.285	114.07	496.56
C3[a]	5.686	15.239	6.287	114.20	496.91
C4[a]	5.710	15.278	6.296	115.52	495.71
C8[a]	5.823	15.281	6.341	118.79	494.57
C9	5.820	15.268	6.327	118.44	494.38
C10	5.846	15.215	6.338	118.78	494.16
C11	5.839	15.207	6.341	118.65	494.12
C12	5.832	15.203	6.357	118.78	494.01

(a) The lattice parameters of the precipitates C3, C4, and C8 were calculated using exclusively the reflections assigned to intermediate members of the solid solution (see text).

The diffractograms of precipitates C5, C6 and C7 have some peculiarities that allow us to identify them as an ardealite-type phase. In these three cases, the largest spacing in the diffraction pattern occurs at ~7.75 Å, a value significantly larger than those of the end-members brushite and gypsum (at ~7.58 and ~7.60 Å, respectively). This reflection is rather sharp, appears isolated (see Fig. 2) and can be attributed to the typical 040 spacing of natural ardealite and "ardealite-like" synthetic compounds[23]. The occurrence of 0*k*0 reflections with $k = 4n$ only (040, 080, and 0160 at ~7.75, 3.88, and 1.94 Å) indicates that the periodicity along the *b*-axis occurs at four times the elementary stacking layer, as described previously. Some typical broad peaks caused by the occurrence of several reflections at very close 2θ angles (e.g. $\bar{1}12$ and 111 at 28.85º and 28.86º), as well as the presence of peaks at ~2.81, 2.54, and 2.45 Å (indexed as $\bar{2}21$, 200, and 062 using a *C*1*c*1-setting), are also typical of ardealite. Moreover, there are several reflections in C5, C6 and C7 that are missing in the pattern calculated by Sakae and co-workers[25] but are usually observed in natural ardealite[40].

In the structure of the synthetic ardealite obtained by Sakae and co-workers[25], there are two types of tetrahedral positions that occur in alternating (040) layers that are linked by hydrogen bonds from water molecules. In a first approach, these two different tetrahedral positions could be considered to be occupied alternatively by phosphorous and sulfur. However, the single-crystal X-ray data indicate that the SO_4^{2-}/HPO_4^{2} distribution is not ordered. In the model by Sakae and co-workers[25] all of the elementary contrasting layers are chemically analogous and thus comparable to the contrasting layers of brushite and gypsum. However, the mode of stacking occurs in such a way that the repeating period includes four layers. Here, the relatively sharp 040 reflection in diffractograms C5, C6, and C7 allows us to play down the occurrence of compositional heterogeneities and support the existence of an ardealite-type layering in these precipitates with a composition close to $Ca_2SO_4HPO_4{\cdot}4H_2O$. Note that if we choose $a < c$ (5.721 < 6.250 Å) for the

unit cell of ardealite, the space group setting will be $C1c1$, whereas if we choose $a > c$ (6.250 > 5.721 Å), the space group will be $A1a1$. This is the inverse of the case of brushite and illustrates again that, despite the structural similarities, the ardealite structure[25] does not correspond to a member of the $Ca(SO_4,HPO_4)\cdot 2H_2O$ solid solution. Moreover, despite the double *b*-axis parameter (lower translational symmetry) the ardealite structure cannot be considered a superstructure of the "basic" brushite structure.

Table 3 shows the composition, expressed as the brushite mole fraction (X_{br}), of the phases obtained in the whole set of precipitation experiments. These compositions were determined from the difference between the initial and final concentrations of sulfate and phosphate in the aqueous solution. The composition was also checked by SEM-EDS microanalysis of the solids, and the results were in good agreement (the deviation was less than 0.03 X_{br}) with those calculated from analyses of the aqueous solution. The nature of the solid phases involved is also shown in Table 3. In the case of experiments C3, C4, and C8, the precipitates were heterogeneous mixtures whose diffractograms show two reflections in the region of largest spacings (see Fig. 2). The first reflection (at ~7.75 Å) corresponds to the 040 spacing of an ardealite-like compound, and the second can be attributed to the 020 spacing (~7.60 Å) of a member of the $Ca(SO_4,HPO_4)\cdot 2H_2O$ solid-solution. Thus, as shown in Table 3, two phases (a disordered solid solution and an ardealite-type compound with $X_{br} \approx 0.5$) were simultaneously obtained from these parent solutions. The set of reflections unequivocally assigned to the solid solution can be used to refine their lattice parameters using X'Pert HighScore Plus. These parameters have been included in Table 2 (see C3, C4, and C8) together with those of the homogeneous precipitates (C1, C2, C9, C10, C11, and C12). Unfortunately, the composition of the solid-solution phase in the C3, C4 and C8 mixtures is uncertain, as the chemical analyses involve two phases. Moreover, the unit cell dimensions do not vary in a linear way with composition and cannot be used to make more than a very rough estimation.

Table 3. Composition and nature of the phases obtained in the precipitation experiments.

Sample	X_{br} (± 0.02)	Phase(s)
C1	0	gypsum end-member
C2	0.09	solid solution
C3*	?	ardealite + s.s.
C4*	?	ardealite + s.s.
C5	0.46	ardealite
C6	0.56	ardealite
C7	0.59	ardealite
C8*	?	ardealite + s. s.
C9	0.87	solid solution
C10	0.91	solid solution
C11	0.93	solid solution
C12	1.00	Brus. end-member

(a) The composition of the solid-solution phase (s.s.) in the C3, C4 and C8 mixtures could not be measured (see text). A rough estimation from the unit cell dimensions is given in text.

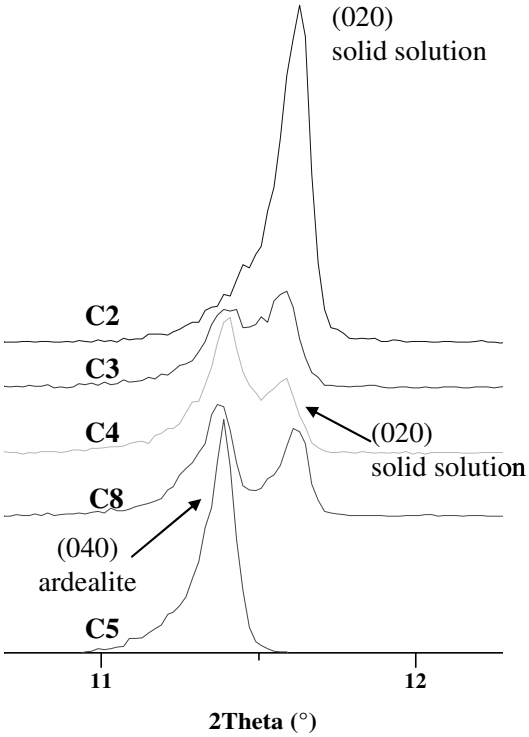

Figure 2. Detail of the region of largest spacings in the powder diffraction patterns of C2, C3, C4 and C5. In C2, the reflection 020 appears isolated. C3, C4 and C8 are mechanical mixtures of ardealite with a $Ca(SO_4,HPO_4)\cdot 2H_2O$ solid-solution member (reflections 040 and 020, respectively). In C5, only an ardealite phase appears (reflection 040).

The appearance of two ranges of "mechanical mixtures" denotes the existence of two miscibility gaps, one on each side of the "ardealite-range" of compositions. This further supports the idea of attributing a different nature to the solids with compositions $X_{br} \approx 0.5$. The homogeneous solids ($0.46 \leq X_{br} \leq 0.59$) obtained in C5, C6, and C7 cannot be considered members of the solid solution, as their diffractograms match with a (040)-layered ardealite-type compound[25]. Unfortunately, while the presence of two gaps is clearly demonstrated in experiments C3, C4, and C8, the equilibrium miscibility limits are difficult to establish. In the $X_{br} < 0.5$ range, the solid solution in the C4 mixture can be expected to be the most phosphate-rich member obtained in the present experiments. According to the general trend of the cell parameters (see Table 2), this sample could correspond to compositions of approximately $X_{br} \approx 0.15$. However, as the precipitation experiments were carried out at a high supersaturation, a solid solution with this composition could be metastable, and the thermodynamic range of miscibility could be narrower. Similarly, in the $X_{br} > 0.5$ range, the most sulfate-rich member occurs in C8 and could correspond to compositions of approximately $X_{br} \approx 0.85$. Finally, the ardealite-type 040 spacings observed for C3, C4 and C8 fall in the 7.76-7.75 Å range, which indicates that the compositions observed for these (stable or metastable) ardealite-type phases do not exceed the limits $0.46 \leq X_{br} \leq 0.59$.

3.2. Excess volume of mixing

Figure 3a displays the value of the crystallographic parameter *b* for the solids obtained in the experiments compiled in Table 2. The data-point labels indicate the solid composition expressed as mole fraction of brushite (X_{br}). As shown in this figure, for intermediate compositions, all data fall above the straight line that connects the values corresponding to the pure gypsum and brushite end-members (C1 and C12). At first sight, this result seems to indicate the existence of a positive excess volume of mixing (ΔV^{ex}) in the solid solution. The excess volume of mixing is defined as the difference between the molar volume of the solid solution (V_{SS}) and the molar volume of a mechanical mixture (V_{MM}) of the end-members with the same composition (X_{br}) according to the expression:

$$\Delta V^{ex} = V_{SS} - [V_{br} X_{br} + V_{gy} X_{gy}] \quad (1)$$

where the quantity in brackets corresponds to V_{MM} and the terms V_{br} and V_{gy} are the molar volumes of pure brushite and gypsum, respectively. Clearly, $X_{gy} = 1\text{-}X_{br}$ is the molar fraction of the gypsum component in the solid solution. The molar volume of the solid solution (V_{SS}) can be determined from the unit cell volume (V_{cell}) using the expression:

$$V_{SS} = \frac{1}{4} V_{cell} N_{Avogadro} \quad (2)$$

where the factor 1/4 arises from the four formula units contained in the unit cells of gypsum and brushite. The molar volumes of the brushite and gypsum end-members (74.37 and 74.59 cm^3 mol^{-1}) were also derived from the corresponding unit cell parameters. The values of V_{SS}, V_{MM}, and ΔV^{ex} calculated in this way are shown in Table 4 where it is obvious that the excess volume of mixing is clearly positive, but very small. In reality, the expansion of the unit cell along the *b* axis observed for intermediate compositions is accompanied by a significant deformation of the unit cell shape on the (010) plane. The unit cell parameters *a* and *c* vary in an irregular way with the composition (increase for some ranges and decrease for others), and the β-angle is significantly higher for the P-rich members than for the S-rich members.

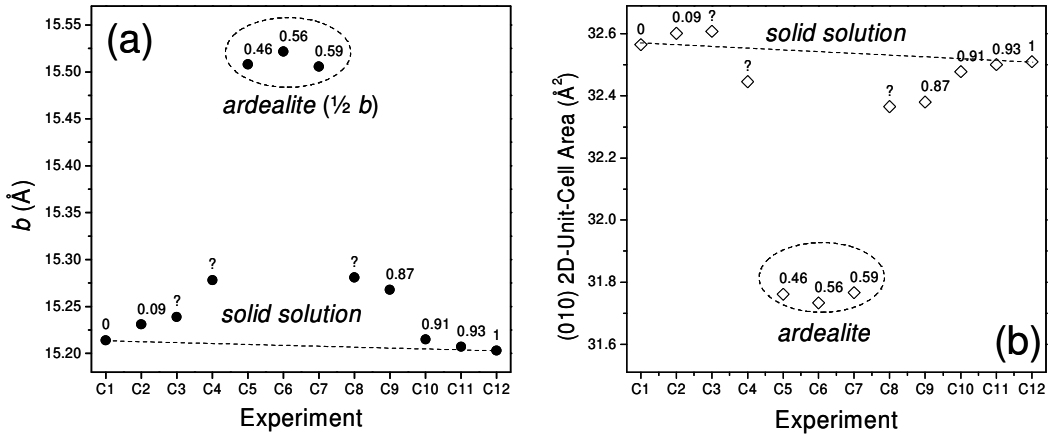

Figure 3. a) Values of the unit cell parameter *b* for the complete experimental series. The labels near the data points indicate the solid composition (X_{br}). The three data points encircled by a dashed line correspond to the ardealite phase obtained in experiments C5, C6, and C7 and represent one-half of the repeating period along the *b*-axis (see text). The rest of the data correspond to different members

of the $Ca(SO_4,HPO_4)\cdot 2H_2O$ solid solution. b) Area of a two-dimensional unit cell on (010). Again, the data points encircled by a dashed line correspond to an ardealite-type phase.

Figure 3a also displays (encircled by a dashed line) three data points corresponding to experiments C5, C6, and C7. These three values represent one-half of the repeating period along the *b*-axis ($2\times d_{040}$) and have been plotted to illustrate the dilatation of the interlayer spacing in ardealite as compared to the solid-solution members. It is worth noting that the values of ΔV^{ex} obtained using Eqn. (1) for experiments C5, C6, and C7 are clearly negative (≈ -0.35 cm^3/mol). These values are meaningless, as they correspond to a solid phase whose structure is not equivalent to that of the solid solution. However, they still indicate that, in ardealite, while the interlayer spacing is expanded, the (040) layers are dramatically contracted when compared with the equivalent (020) layers of pure gypsum and brushite. This phenomenon is illustrated in Fig. 3b, which displays the area of a two-dimensional unit cell on (010) as a function of composition. As shown in this figure, the incorporation of sulfate ions into the brushite structure leads to a contraction of the (020) layers. In contrast, on the sulfate-rich range, the incorporation of phosphate substituting for sulfate initially produces a positive deviation in the 2D unit cell area. Therefore, the SO_4^{2-}/HPO_4^{2-} substitution does not produce a symmetric effect on both miscibility ranges. Finally, precipitates C5, C6 and C7 exhibit a strongly differentiated behavior and are plotted below to form a separated population labeled as ardealite in Fig. 3b.

3.3. Enthalpy of precipitation and enthalpy of mixing

In a similar way to ΔV^{ex}, the excess enthalpy of mixing (ΔH^{ex}) is given by the difference between the enthalpy of the solid solution (H_{SS}) and the enthalpy (H_{MM}) of a mechanical mixture of the end-members with the same composition. The excess enthalpy of mixing can be determined from the calorimetric data (see section 2.1) obtained during the precipitation experiments, according to the expression below[39]:

$$\Delta H^{ex} = H_{SS}^{ppt} - H_{MM}^{ppt} \quad (3)$$

where H_{SS}^{ppt} stands for the measured enthalpy of precipitation of a solid solution of composition X_{br} and H_{MM}^{ppt} is the enthalpy of precipitation of a compositionally equivalent mechanical mixture of the pure brushite and gypsum end-members, given by:

$$H_{MM}^{ppt} = H_{br}^{ppt} X_{br} + H_{gy}^{ppt} X_{gy} \quad (4)$$

In this equation, H_{br}^{ppt} and H_{gy}^{ppt} are the measured enthalpies of precipitation of the pure brushite and gypsum, respectively. Table 4 displays the values of the precipitation enthalpy (H^{ppt}) obtained from the calorimetric measurements carried out during experiments C1, C2, C9, C10, C11, and C12. Each value corresponds to the average of five replicate experimental runs. The relative standard deviation (RSD) in H^{ppt} was approximately ±6%, which is a relatively small margin of error. As can be observed in Table 4, while the enthalpy of precipitation of gypsum is significantly lower than that of brushite, the values obtained for the intermediate compositions of the solid solution are all close to 2.5 kJ/mol. As a consequence, the excess enthalpy of mixing calculated according to Eqn. (3) is clearly negative for the phosphate-rich members ($X_{br} > 0.85$) and slightly positive in the sulfate-rich ($X_{br} < 0.15$) miscibility range. The values corresponding to C3, C4 and C8 are not displayed in Table 4 because these experiments involve an assemblage of two phases. Similarly, the values for C5, C6, and C7 have been excluded from Table 4 because they correspond to ardealite-type phases. Obviously, we can use Eqn. (3) to calculate the values of ΔH^{ex} for these precipitates (≈–1.6 kJ·mol^{-1}), but the physical meaning is uncertain because ardealite has a different structure, enthalpy and entropy than a compositionally equivalent solid solution.

Table 4 Excess volume (ΔV^{ex}) and enthalpy (ΔH^{ex}) of mixing. The molar volumes of the precipitated solid solutions (Vss) and those of a mechanical mixture (V_{MM}) of the end-members with the same composition are also shown. The last two columns display the enthalpy of precipitation (H^{ppt}) and excess enthalpy of mixing obtained from the calorimetric measurements.

Experiment	X_{br} (± 0.02)	V_{SS} (cm^3/mol)	V_{MM} (cm^3/mol)	ΔV^{ex} (cm^3/mol)	H^{ppt} (kJ/mol)	ΔH^{ex} (kJ/mol)
C1	0	74.590	74.590	-	1.09 ± 0.13	-
C2	0.09	74.757	74.570	0.186	2.51 ± 0.41	0.92
C9	0.87	74.429	74.402	0.028	2.62 ± 0.39	-3.13

C10	0.91	74,395	74.393	0.002	2.65 ± 0.37	-3.31
C11	0.93	74.429	74.389	0.003	2.57 ± 0.12	-3.54
C12	1.00	74.373	74.373	-	6.46 ± 1.46	-

The negative value of the excess enthalpy of mixing in precipitates C9, C10, and C11 is in agreement with the contraction of the (020) layers, shown in Fig. 3b. Both effects seem to indicate that, in the phosphate-rich range, the substitution of HPO_4^{2-} by SO_4^{2-} increases the bond interaction within these layers. In the simplest case, a negative enthalpy of mixing correlates with a negative excess volume of mixing (i.e., with a contraction of the structure) and implies a tendency toward alternation (ordering) of the substituting ions[41]. Here, such a tendency can be expected to occur within each (020) layer and does not imply SO_4^{2-}/HPO_4^{2-} ordering in alternating layers as the layer spacing expands. Moreover, the ardealite-type structure determined by Sakae and co-workers[25] does not exhibit any sign of SO_4^{2-}/HPO_4^{2-} ordering. The existence of a negative enthalpy of mixing does not necessarily imply the stability of the ordered phase due to its lower entropy. Moreover, ordering is frequently precluded by the crystallization kinetics. In practice, the strong contraction of the (020) layers seems to resolve in a different stacking sequence (with double *b*-axis parameter) for the ardealite range of compositions.

3.4. Phase distribution scheme

Although a precise determination of the degree of non-ideality of the $Ca(SO_4,HPO_4)\cdot 2H_2O$ solid solution was not possible, the existence of two miscibility gaps, one on each side of the ardealite range of compositions, is clearly related to the tendency to form a "double salt". Further, the existence of these two gaps reinforces the idea that ardealite is not a member of the brushite-gypsum solid solution. The fact that slightly different diffraction patterns have been observed for ardealite-type phases is not strange. In layered compounds with complex stacking sequences like ardealite, the presence of stacking faults and/or different polytypes[42] is always a possibility and would explain the observed phenomena.

The occurrence of intermediate, ordered phases coexisting with miscibility gaps is frequent in nature. Such is the case of the formation of ordered dolomite $CaMg(CO_3)_2$ as an intermediate phase (with double *c*-axis parameter) in the $CaCO_3$-$MgCO_3$ system. In these cases, ordering and unmixing are closely related and interdependent phenomena, and their relative kinetics is decisive in defining the result at specific conditions. These systems have certain similarities with the $CaSO_4{\cdot}2H_2O$-$CaHPO_4{\cdot}2H_2O$ system, even though the available structural data[25] suggest that the SO_4^{2-}/HPO_4^{2-} distribution is random. A crucial point is that the ardealite structure shows a (040) layering that involves two topologically different types of tetrahedral positions. This stacking sequence only appears for the midterm composition, probably as a result of the strong contraction of the stacking layers. Finally, the observation that the SO_4^{2-}/HPO_4^{2-} substitution does not produce symmetric effects (see Fig. 3b and ΔH^{ex} values in Table 4) on both miscibility ranges is not strange. Brushite and gypsum are not completely isostructural due to the different orientation of the tetrahedra and to the presence of the acidic hydrogen in the phosphate group. The brushite structure exhibits a chain of hydrogen bridges that connects adjacent HPO_4^{2-} tetrahedra along [101], which is clearly absent in gypsum. Thus, on the phosphate-rich side, the substitution of HPO_4^{2-} by SO_4^{2-} will involve the cancelation of some H-links in these chains and a local, energetically favorable reorientation of the tetrahedra.

Figure 4 displays a schematic model that qualitatively represents the phase relationships in the gypsum-brushite system. The scheme defines the compositional fields where either single phases or assemblages of two phases exist. A single solid solution phase is stable within two compositional regions, I and V, whereas ardealite is stable within III. There are two compositional intervals (II and IV) where assemblages of ardealite and the solid solution are stable. The first, (II), corresponds to a mixture of an ardealite phase with composition x_2 and a solid solution with composition x_1. The second, (IV), corresponds to the assemblage of an ardealite phase with composition x_3 and a solid solution with composition x_4. As can be observed, the regions defined in Fig. 4 correspond to the compositional fields defined by the precipitation experiments presented in this work (Table 3).

However, the extent of these experimental regions most likely does not reflect the true stability limits, as precipitation occurred far from equilibrium, and the obtained limits could involve metastable compositions. Figure 4 also displays a projection of a 101 slice of the crystal structures of ardealite as well as a phosphate-rich and a sulfate-rich member of the solid solution in which the different repeating periods along the *b*-axis can be observed.

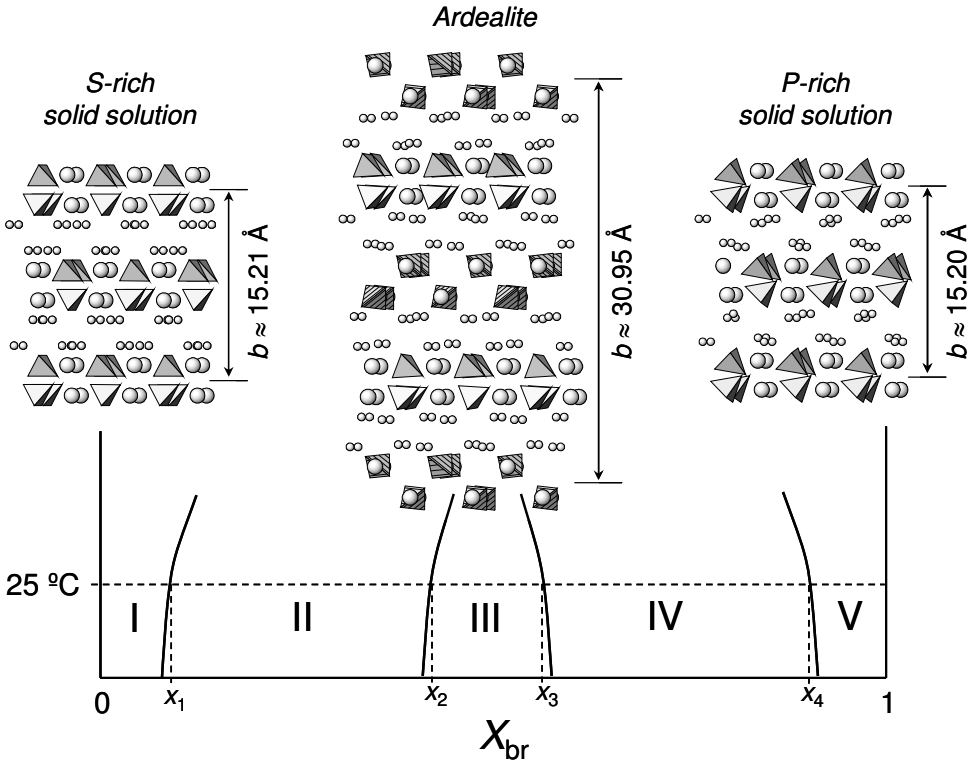

Figure 4. Scheme of the distribution of phases in the $CaSO_4 \cdot 2H_2O$-$CaHPO_4 \cdot 2H_2O$ system. The figure also shows the projection of 101 slices of the structures of ardealite ($Ca_2SO_4HPO_4 \cdot 4H_2O$) and of the two extremes of the $Ca(SO_4,HPO_4) \cdot 2H_2O$ solid solution. In the case of ardealite[24], there are two topologically non-equivalent tetrahedral positions (striped and non-striped tetrahedra in the figure). In all cases, the small circles represent oxygen atoms from the water molecules. The larger circles represent the calcium atoms. Hydrogen atoms are not represented. The solid lines separate the hypothetical stability fields of the different phases described in the text.

3.5. Dehydration behavior of the solid phases in the gypsum-brushite joint

Although previous observations and the available structural data clearly support the view that ardealite is not a member of the $Ca(SO_4,HPO_4) \cdot 2H_2O$ solid solution, studies of the dehydration behavior of the solids obtained in these experiments can provide further insight into this matter.

With this aim, Figures 5 through 9 show the results of a dehydration study carried out by combining thermogravimetric and thermo-XRD techniques.

Figure 5 displays the thermogravimetric (TG) (weight loss as a function of temperature) and the derivative thermogravimetric (DTG) curves obtained for gypsum (Fig. 5a), brushite (Fig. 5b), a sulfate-rich member (Fig. 5c), and a phosphate-rich member (Fig. 5d) of the $Ca(SO_4,HPO_4)\cdot 2H_2O$ solid solution. There is a reduction of approximately 21% of the initial weight in all of the samples, which corresponds to the total loss of two water molecules per formula unit. However, the DTG curves show that this process occurs in a different way for brushite-rich and gypsum-rich members of the solid solution. As expected, the dehydration of the pure-gypsum sample C1 involved an initial loss of ~75% of water molecules (Fig. 5a), which was attributed to formation of bassanite ($CaSO_4\cdot 0.5H_2O$). This initial loss was followed by complete dehydration to form anhydrite (γ-$CaSO_4$) at approximately 150ºC. In contrast, the pure-brushite sample C12 (Fig. 5b) dehydrates in a single step at ~125ºC to form monetite (anhydrous $CaHPO_4$). This temperature is lower than the typical values (150–180ºC) reported in the pioneering XRD[35], which could be due to the effect of using different heating rates, grain sizes, and impurities on the kinetics of the dehydration process.

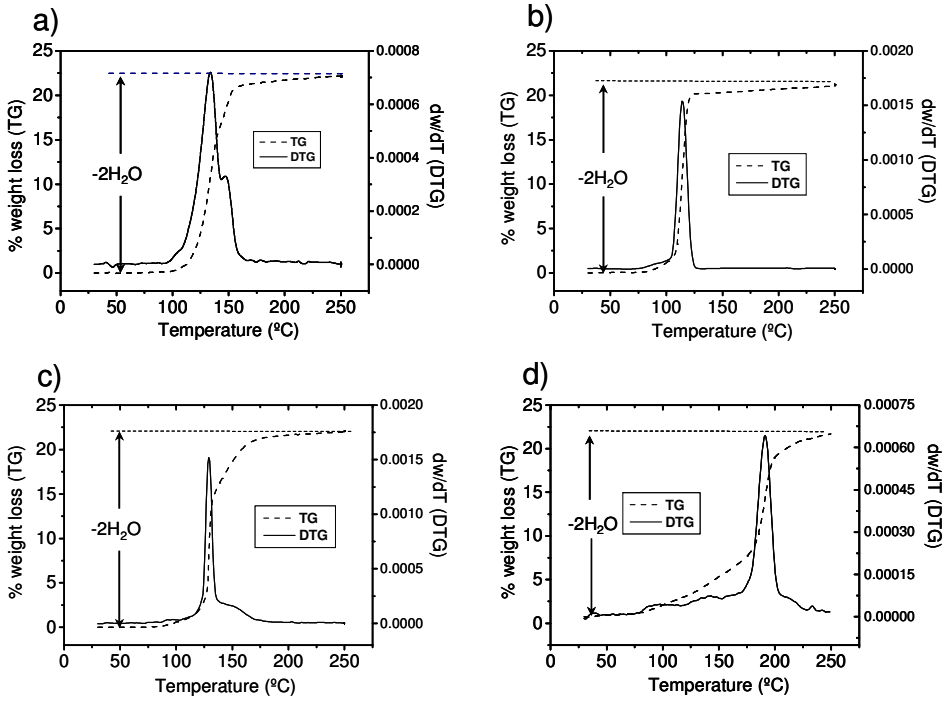

Figure 5. Thermogravimetric (TG) and derivative thermogravimetric (DTG) curves determined for gypsum (a), brushite (b), a sulfate-rich (c) and a phosphate-rich (d) member of the $Ca(SO_4,HPO_4)\cdot 2H_2O$ solid solution.

The solid-solution sample representative of sulfate-rich compositions (C2) exhibits a similar behavior to that observed for gypsum (Fig. 5c), with completion of the dehydration process at ~160ºC. The only difference with respect to pure gypsum is that the two dehydration steps are less individualized (see the small shoulder on the right side of the curve) so that the DTG curve simply reflects a decrease in the rate of dehydration after the initial loss of 75% of the water molecules. In contrast, the dehydration of the phosphate-rich sample C10 (Fig. 5d) occurs in a single step, as it does in brushite, although at significantly higher temperatures (~200ºC) than in the case of the pure brushite end-member. Moreover, there is a weight loss of approximately 7.5% before the dehydration peaks of the DTG curve (see the left side of the TG curve in Fig. 5d). From these observations, one can assume that the sulfate and the phosphate-rich members of the solid solution tend to emulate the dehydration behavior of the respective pure end-members, albeit with some differences. Specifically, it seems that the presence of sulfate ions dramatically increases the dehydration temperature of brushite.

The TG and DTG curves displayed in Fig. 6 correspond to the dehydration of the ardealite-type phase obtained in C5. As can be observed, for ardealite, the completion of the water loss occurs at higher temperatures (~250ºC) than in the case of brushite and gypsum. Moreover, the process occurs in two steps, each involving ~50% loss of water molecules. Both of these observations support the idea that ardealite exhibits a distinctive behavior and cannot be considered a member of the $Ca(SO_4,HPO_4)\cdot 2H_2O$ solid solution. The nature of the phases resulting from the two dehydration steps, however, requires further research. Toward this aim, a thermo-XRD study is likely the best tool to complement the macroscopic TG-DTG analyses and to identify the dehydration products.

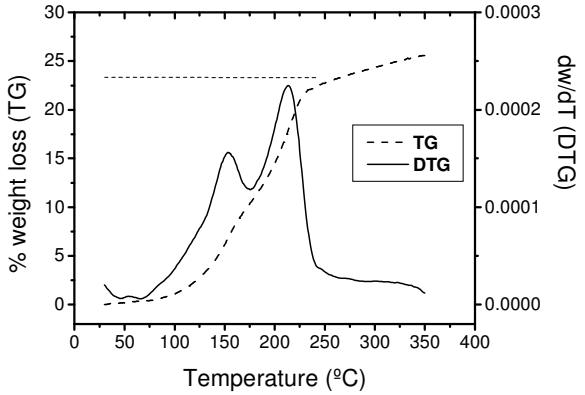

Figure 6. Thermogravimetric (TG) and derivative thermogravimetric (DTG) curves determined for the ardealite sample C5.

Fig. 7 displays a series of diffractograms obtained at different temperatures, starting from the sulfate-rich member of the $Ca(SO_4,HPO_4)\cdot 2H_2O$ solid solution synthesized in experiment C2 (X_{br} = 0.09). This member shows a gypsum-type structure (see Table 2 in section 3.1), with displacement of the reflections toward smaller 2θ angles than in the case of pure gypsum caused by the SO_4^{2-}/HPO_4^{2-} substitution. When the temperature increases up to ~110–120ºC, some new peaks in the diffraction pattern occur together with the pre-existing gypsum peaks. These new reflections can be identified as belonging to bassanite ($CaSO_4\cdot 0.5H_2O$) and/or γ-anhydrite (γ-$CaSO_4$). With increasing temperature, the typical reflections of gypsum progressively disappear so that, in agreement with the TG-DTG observations, at 150ºC, the dehydration process is virtually completed, and only metastable γ-anhydrite seems to be present. It is worth noting that the crystal structures of bassanite and γ-anhydrite show only slight differences related to the presence (or not) of water molecules[32,43]. Therefore, discrimination between both phases is not straightforward using conventional powder XRD. However, we assume that the diffractogram taken at 150ºC corresponds to γ-anhydrite, as the TG-DTG curves indicate that complete dehydration is attained at this temperature. No sign of any phosphate phase has been detected, which seems to indicate that SO_4^{2-}/HPO_4^{2-} substitution can still occur in the anhydrous residuum.

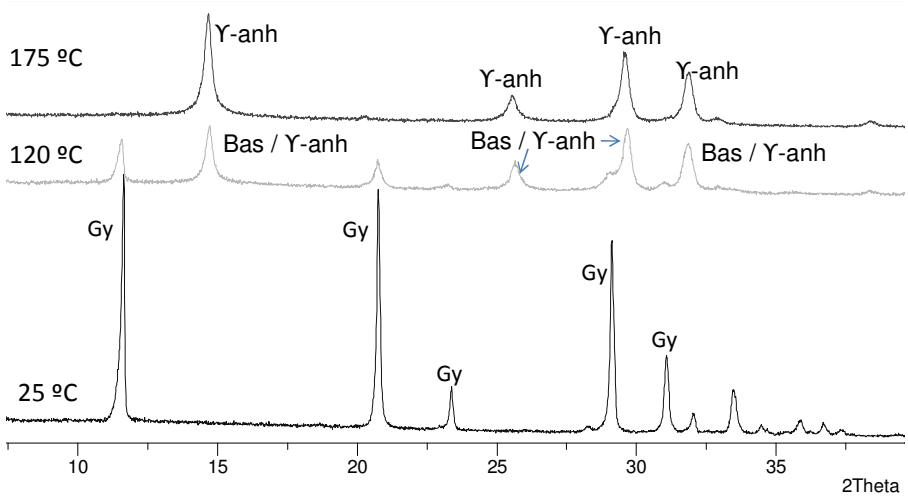

Figure 7. Powder XRD patterns obtained during the dehydration of a sulfate-rich member of the $Ca(SO_4, HPO_4)\cdot 2H_2O$ solid solution (C2).

Figure 8 depicts a series of XRD patterns that correspond to the dehydration products of a phosphate-rich member (C10) of the $Ca(SO_4,HPO_4)\cdot 2H_2O$ solid solution (X_{br} = 0.91). The first diffractogram (taken at 25ºC) can be attributed to a brushite-type structure (see section 3.1) with a slight displacement of the reflections toward smaller 2θ angles than those corresponding to the pure brushite end-member. At ~150ºC, two peaks (at $d \approx 3.37$ and 3.35 Å) develop to occur together with the brushite reflections. This doublet clearly corresponds to the most intense peaks of monetite ($CaHPO_4$), which indicates that dehydration (accompanied by a gradual decrease of crystallinity) begins at this temperature. Beyond 170ºC, the brushite peaks progressively lose expression, and the monetite reflections become dominant to be the only detectable in the diffractograms taken at temperatures greater than 190ºC. These results reveal a notable similarity between the dehydration mechanisms of brushite and of phosphate-rich members of the $Ca(SO_4,HPO_4)\cdot 2H_2O$ solid solution. Because the identified dehydration products of these precipitates consist only of monetite (no sulfate phase has been detected), some SO_4^{2-}/HPO_4^{2-} substitution can be expected in the structure of monetite. An alternative would be the concentration of sulfate in an anhydrous residuum of low-crystallinity, which would simply contribute to an increased background of the diffractograms.

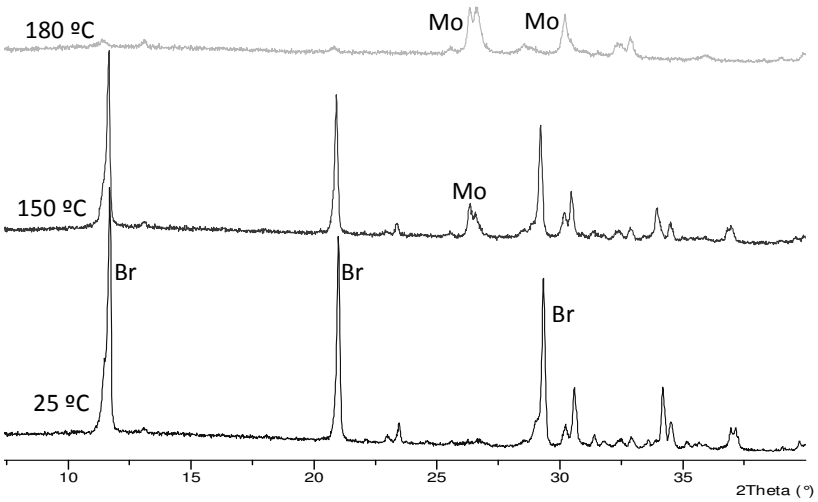

Figure 8. Powder XRD patterns obtained during the dehydration of a phosphate-rich member of the $Ca(SO_4, HPO_4)\cdot 2H_2O$ solid solution (sample C10).

The thermal-XRD evolution of the ardealite-type phase obtained in experiment C5 is shown in Fig. 9, where the typical 040 reflection can be observed. Evidence of dehydration does not appear before 150ºC, when new reflections corresponding to a bassanite-type ($CaSO_4\cdot 0.5H_2O$) and/or an anhydrite-type (γ-$CaSO_4$) phase begin to develop. From 150 to 190ºC, the intensity of the ardealite reflections decreases in a gradual way, and at 200ºC, metastable (γ-$CaSO_4$) anhydrite is the only phase that is identifiable in the diffractograms. Dehydration is accompanied by an important decrease in crystallinity, which becomes evident by the low intensities and high FWHM values observed in the diffractograms of the dehydration product. It is worth noting that crystalline phosphate solids were not detected. Two incipient reflections reminiscent of the typical doublet observed in monetite were detected in some diffractograms (see Fig. 9), but this occurrence cannot be considered significant given the high phosphate content (50 mole percent) of ardealite. Overall, the thermal-XRD data are consistent with a dehydration process that proceeds toward an anhydrite-type material embedded in an almost amorphous residuum. The low degree of crystallinity would favor the incorporation of phosphate substituting for sulfate in the molecular framework of this dehydration product. Above ~250ºC, the diffractograms develop two incipient reflections at $d \approx$ 3.50 and 2.85 Å. Finally, as the temperature increases from 300 to 450ºC, these two reflections gain

definition (particularly the one at 3.50 Å) and become clearly indicative of the presence of β-$CaSO_4$, the stable structural variant of anhydrite. In fact, the two most intense reflections (020 and 012) in the β-$CaSO_4$ reference diffractogram occur exactly at 3.4988 Å and 2.8494 Å, respectively. This finding seems to indicate a gradual transformation from metastable anhydrite (γ-$CaSO_4$) to stable anhydrite (β-$CaSO_4$) when the temperature increases to within this range.

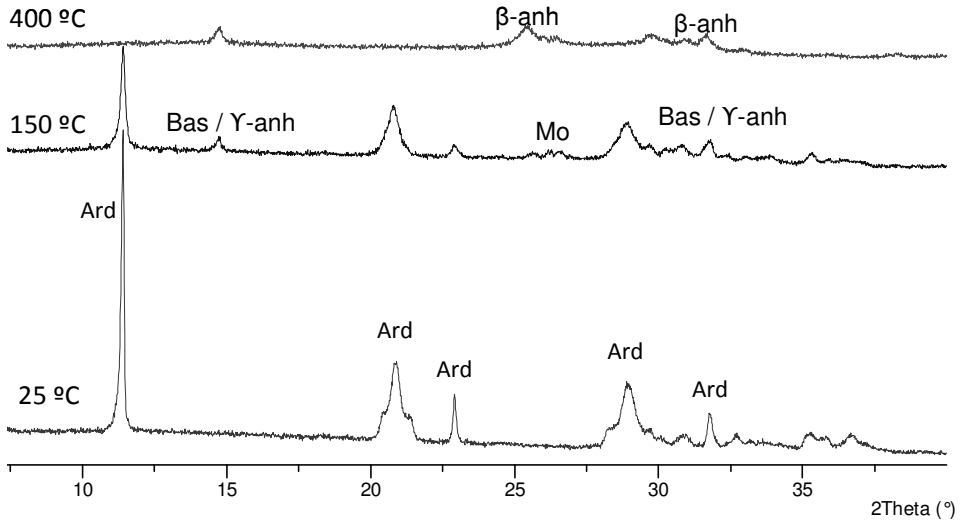

Figure 9. Powder XRD patterns obtained during the dehydration of ardealite $Ca_2SO_4HPO_4{\cdot}4H_2O$ (sample C5).

The previous results indicate the existence of three different dehydration behaviors in the $CaSO_4{\cdot}2H_2O$-$CaHPO_4{\cdot}2H_2O$ system. For both the sulfate-rich and the phosphate-rich member of the solid solution, the macroscopic (TG-DTG) study and the XRD data match rather well. However, for ardealite, the correlation between the TG-DTG curves and the sequence of phases observed in the thermo-XRD study is not straightforward. Whereas the DGT curve indicates that the water loss occur in two steps, distinguishing two singular events (each equivalent to a 50% water loss) from the sequence of diffractograms taken at increasing temperatures proves impossible. Moreover, although the ardealite reflections vanish completely at 200ºC, according to the DTG curves, the dehydration proceeds to a temperature of 250ºC, and the sample continues to lose weight beyond this temperature. A reasonable speculation could be the preferential dehydration of the gypsum

$CaSO_4 \cdot 2H_2O$ component of ardealite to form bassanite, γ-anhydrite and a low-crystallinity residuum that is rich in the brushite $CaHPO_4 \cdot 2H_2O$ component. In a second step (see Fig. 6), this residuum could dehydrate to form a $CaHPO_4$-rich phase of low crystallinity. Finally, further loss of water molecules (at T > 250ºC) could occur by means of the following reaction[40]:

$$2CaHPO_4 + 2\gamma CaSO_4 \rightarrow Ca_2P_2O_{7\,(amorphous)} + 2\beta CaSO_4 + H_2O \qquad (5)$$

In this reaction, an amorphous $Ca_2P_2O_7$ phase would become the target store for most of the initial phosphorous content of ardealite.

4. CONCLUSIONS AND FUTURE WORK

Although the crystal chemistry and mixing properties in the gypsum-brushite joint need further clarification, the foremost significance of our findings is the consistency of the conclusions obtained through different methods of analysis. For example, the existence of a negative enthalpy of mixing in the phosphate-rich miscibility range is consistent with the contraction of the (020) layers with respect to the pure brushite. Both effects point toward a reinforcement of the structure when SO_4^{2-} substitutes for HPO_4^{2-}, which in turn is in agreement with the significant increase of the dehydration temperature (compare Figs. 5b and 5d) observed in the thermogravimetry experiments. At the end, the contraction of the (020) layers resolves in a different stacking sequence (with a double *b*-axis parameter) for the ardealite range of compositions. This structural change confers a special nature to ardealite, which cannot be considered a member of the $Ca(HPO_4,SO_4) \cdot 2H_2O$ solid solution. The TG-DTG curves indicated a specific dehydration behavior for the ardealite samples, which again supports the guess that this phase is not a member of the solid solution. Finally, the conclusion that the tendency to order does not imply an HPO_4/SO_4 alternation in the stacking layers is revealing. Though all the stacking layers are chemically identical, the lack of equivalence between tetrahedral positions of alternating layers appears to be a stacking (topological) effect.

There are, however, several issues that require further study. Whereas the existence of a tendency to HPO_4/SO_4 ordering within each (040) layer has been proved, ardealite appears to be

disordered. Doubt persists whether this disorder is a thermodynamic or a kinetic effect. Moreover, the mechanism of contraction (the local rearrangement of tetrahedra when sulfate substitute for phosphate) remains unknown. Molecular simulations and single-crystal diffraction could help to answer these questions. Finally, an evaluation of the geochemical significance of the gypsum-brushite system would require determining the solubility of ardealite and different members of the solid solution. Future work will address these matters.

AKNOWLEDGEMENTS

This research was supported by the Marie Curie European Network "Mineral Nucleation and Growth Kinetics" (European Commission grant UE-MRTN-CT- 2006- 035488) and by the Spanish Ministry of Education and Science (grant CGL2010-20134-CO2-02). We thank two anonymous referees and A. V. Mudring for the constructive comments that have helped to improve the overall quality of our paper.

Supporting Information. SEM image and EDS spectra of a representative solid formed via precipitation experiments. This material is available free of charge via the Internet at http://pubs.acs.org.

REFERENCES

(1) Stipp, S. *Elements* **2008**, *4,* 75-76.

(2) Wang, L.; Nancollas, G.H. *Chem. Rev.* **2008**, *108*, 4628-4669.

(3) Oelkers, E.H.; Valsami-Jones, E. *Elements* **2008,** *4,* 83-87.

(4) Tortet, L.; Gavarri, J.R.; Musson, J.; Nihoul, G.; Sarychev, A.K. *J. Solid State Chem.* **1999**, *141*, 392-403.

(5) Valsami-Jones, E. (2001) *Mineral. Mag.* **2001**, *65*, 611-620.

(6) Kordlaghari, M.P.; Rowell, D.L. *Geoderma*, **2006,** *132*, 105-115.

(7) Arsic, J.; Kaminski, D.; Poodt, P.; Vlieg, E. *Phys. Rev. B* **2004***, 69*, 245406.

(8) Francis, M.D.; Webb, N.C. *Calcif. Tissue Res.*, **1971**, *6*, 335-342.

(9) Johnsson, M.S.A.; Nancollas, G.H. *Crit. Rev. Oral Biol. Med.* **1992**, *3*, 61-82.

(10) Nriagu, J.O. In *Phosphate minerals*, Nriagu, J.O., Moore P.B., Eds.; Springer-Verlag, Heidelberg, 1984, chapter 1, pp. 1- 136.

(11) Fixen, P.E.; Ludwick, A.E.; Olsen, S.R. *Soil Sci. Soc. Am. J.* **1983**, *47*, 112-117

(12) Fiore, S.; Laviano, R. *Am. Mineral.* **1991,** *76*, 1722-1727.

(13) Gillerman, V.S.; Bennett, E. H. *Proc. 32nd Annual Forum on the Geology of Industrial Mineral*. Wyoming State Geol. Surv. Public Info Circ. **1997**, *38*, 207-218.

(14) Schadler, J. *Zb Mineral*. **1932**, *A*, 40-41.

(15) Prieto, M.; Fernández-González, A.; Martín-Díaz, R. *Geochim. Cosmochim. Acta* **2002**, *66*, 783-795.

(16) Andara, A.J.; Heasman, D.M.; Fernández-González, A.; Prieto, M. *Cryst. Growth Des.* **2005***, 5*, 1371-1378.

(17) Bruno, J.; Bosbach, D.; Kulik, D.; Navrotsky, A. *A state-of-the-art report*. OECD NEA, Paris, **2007**, 266 pp.

(18) Heijnen, W.M.M.; Hartman, P. *J. Cryst. Growth* **1991,** *108,* 290-300.

(19) Hina, A.; Nancollas, G.H.; Grynpas, M. *J. Cryst. Growth* **2001**, *223*, 213-224.

(20) Rodríguez-Blanco, J.D.; Jiménez, A.; Prieto, M. *Cryst. Growth Des.* **2007**, *7*, 2756–2763.

(21) Pinto, A.J.; Jimenez, A.; Prieto, M. *Am. Mineral.* **2009**, *94*, 313-322.

(22) Pinto, A.J.; Ruiz-Agudo, E.; Putnis, C.; Putnis, A.; Jimenez, A.; Prieto, M. *Am. Mineral.* **2010***, 95*, 1747-1757.

(23) Rinaudo, C.; Lanfranco, A.M.; Franchini-Angela, M. *J. Cryst. Growth.* **1994**, *142*, 184-192.

(24) Rinaudo, C.; Lanfranco, A.M.; Boistelle, R. *J. Cryst. Growth.* **1996,** *158*, 316-321.

(25) Sakae, T.; Nagata, H.; Sudo, T. *Am. Mineral.* **1978***, 63*, 520-527.

(26) Linck, G.; Jung, H. *Z. Anorg. Allg. Chem.* **1924**, *137*, 407-417.

(27) Strydom, C.A.; Potgieter, J.H. *Thermochim. Acta* **1999**, *332*, 89-96.

(28) Mirwald, P.W. *J. Chem. Phys.* **2008**, *128*, 074502

(29) Bushuev, N.N.; Borisov, V.M. *Russ. J. Inorg. Chem.* **1982**, *27*, 604-609.

(30) Abriel, W. *Acta Cryst. C,* **1983,** *39,* 956-958.

(31) Putnis, A.; Winkler, B.; Fernandez-Diaz, L. *Mineral. Mag.* **1990**, *54*, 123-128.

(32) Lager, G.A.; Armbruster, T.; Rotella, F.J.; Jorgensen, J.D.; Hinks, D.G. *Am. Mineral.* **1984**, *89*, 910-918.

(33) Gallitelli, P. *Periodico Mineral di Roma* **1933**, *4*, 1-42.

(34) Flörke, O. W. (1952). *Neues Jahrb. Mineral. Abh*. **1952**, *84*, 189-240.

(35) McIntosh, A.O.; Jablonski, W.L. *Anal. Chem.* **1956**, *28*, 1424-1427.

(36) Schofield, P.F.; Knight, K.S.; van der Houwen, J.A.M.; Valsami-Jones, E. *Phys. Chem. Miner.* **2004**, *31*, 606-624.

(37) Frost, R.L.; Palmer, S.J.; Pogson, R. *J. Therm. Anal. Calorim.* **2011,** Doi 10.1007/s10973-011-1458-0.

(38) Fernández-González, A.; Andara, A.; Prieto, M. *Cryst. Growth Des.* **2007**, *7*, 545–552.

(39) Katsikopoulos, D.; Fernández-González A.; Prieto, M. *Geochim. Cosmochim. Acta*, **2009**, *73*, 6147-6161.

(40) Balenzano, F.; Dell'Anna, L.; Di Pierro, M.; Fiore, S. *Neues Jahrb. Mineral. Monatsth.* **1984,** *10*, 461-467.

(41) Prieto, M. *Rev. Min. Geochem.* **2009***, 70*, 47-85.

(42) Baronnet, A. *Rev. Min. Geochim.* **1992***, 27*, 231-288.

(43) Ballirano, P.; Maras, A.; Meloni, S.; Caminitu, R. *Eur. J. Mineral.* **2001,** *13,* 985-993.

For Table of Contents Use Only

The link between brushite and gypsum: Miscibility, dehydration and crystallochemical behavior in the $CaHPO_4 \cdot 2H_2O$-$CaSO_4 \cdot 2H_2O$ system

André J. Pinto, Joana Carneiro, Dionisis Katsikopoulos, Amalia Jiménez* and Manuel Prieto.
Dpto. de Geología, Universidad de Oviedo, C/ Arias Velasco s/n, 3305 Oviedo, Spain

The mixing properties of the $Ca(SO_4,HPO_4)\cdot 2H_2O$ solid solution indicate the existence of two ranges of solid solution separated by two miscibility gaps from a range of composition in which the "double salt" ardealite, $Ca_2SO_4HPO_4\cdot 4H_2O$, forms. Calorimetric, crystallographic and dehydration data indicate that ardealite is not a solid-solution member, but a nearly stoichiometric compound with specific structural features.